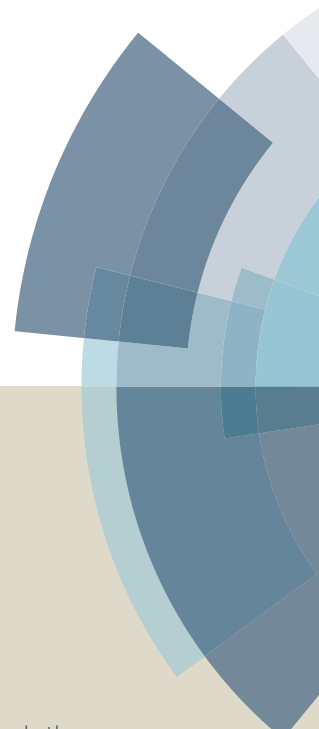
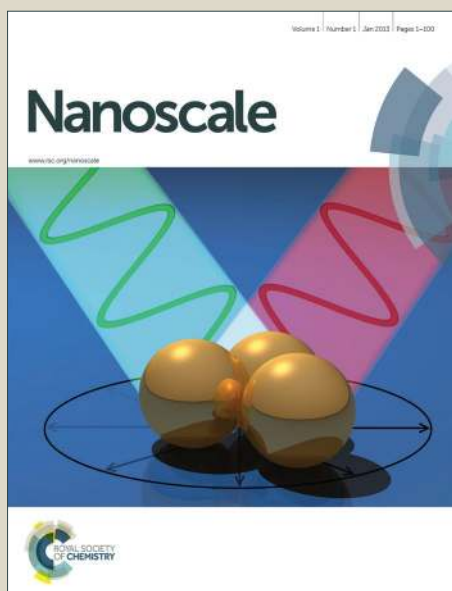


Nanoscale

Accepted Manuscript



This article can be cited before page numbers have been issued, to do this please use: A. S. Melvin, K. Illath, T. Das, R. Thirumalaiswamy, S. Bhattacharyya and G. S. Chinnakonda, *Nanoscale*, 2015, DOI: 10.1039/C5NR03735B.



This is an *Accepted Manuscript*, which has been through the Royal Society of Chemistry peer review process and has been accepted for publication.

Accepted Manuscripts are published online shortly after acceptance, before technical editing, formatting and proof reading. Using this free service, authors can make their results available to the community, in citable form, before we publish the edited article. We will replace this *Accepted Manuscript* with the edited and formatted *Advance Article* as soon as it is available.

You can find more information about *Accepted Manuscripts* in the [Information for Authors](#).

Please note that technical editing may introduce minor changes to the text and/or graphics, which may alter content. The journal's standard [Terms & Conditions](#) and the [Ethical guidelines](#) still apply. In no event shall the Royal Society of Chemistry be held responsible for any errors or omissions in this *Accepted Manuscript* or any consequences arising from the use of any information it contains.



Nanoscale

ARTICLE

M-Au/TiO₂ (M = Ag, Pd, and Pt) Nanophotocatalyst for overall solar water splitting: Role of Interfaces

Ambrose A. Melvin,^a Kavya Illath,^a Tanmay Das,^b Thirumalaiswamy Raja,^a Somnath Bhattacharyya,^b Chinnakonda S. Gopinath^{a,c,d,*}

Received 00th January 20xx,
Accepted 00th January 20xx

DOI: 10.1039/x0xx00000x

www.rsc.org/

M-Au/TiO₂ (M = Ag, Pd, Pt) composites were prepared through a facile one pot photodeposition synthesis and evaluated for solar water splitting (SWS) with and without sacrificial agent. The M-Au combination mimics a dominant character in augmenting the H₂ generation activity by forging into a bi-metallic system. Degussa P25 was used as a TiO₂ substrate to photodeposit Au followed by Au + M (M = Ag/Pd/Pt). SWS activity of the M-Au/TiO₂ was determined through photocatalytic H₂ production in the presence of methanol as sacrificial agent under one sun condition with an AM1.5 filter. The highest H₂ yield was observed for Pt-Au/TiO₂ around 1.3±0.07 mmol/h g, with an apparent quantum yield (AQY) of 6.4 %. Pt-Au/TiO₂ also demonstrated the same activity for 25 cycles of five hours each for 125 h. Critically, the same Pt-Au/TiO₂ catalyst was active in overall SWS (OSWS) without any sacrificial agent with an AQY = 0.8 %. Amount of Au and/or Pt was varied to get the optimum composition and it was found that Pt_{0.5}-Au/TiO₂ composition exhibits the best activity. Detailed characterization by physico-chemical, spectral and microscopy measurements were carried out for an in-depth understanding of the origin of photocatalytic activity of Pt_{0.5}-Au/TiO₂. Above in-depth studies shows that gold interacts predominantly with oxygen vacancies present on titania surfaces, and Pt preferentially interacts with gold for an effective electron-hole pair separation at Pt-Au interfaces and electron storage in metal particles. Pt in Pt_{0.5}-Au/TiO₂ is electronically and catalytically different from Pt in Pt/TiO₂ and it is predicted that the former suppresses the oxygen reduction reaction.

Introduction

Energy is indeed the most vital source for the sustenance of life. It is solar energy that plays an important role for the whole ecosystem on this planet; however, solar energy is not tapped for significant real-world applications yet. Nonetheless, energy derived from fossil fuels play a critical role in supporting and carrying out our day to day activities in life and many industrial activities.¹ Although shale gas/oil is available currently, in addition to the other sources, in general, energy derived from fossil fuels is at stake as there are only limited reserves left. Also, issues related to environmental pollution on using these fossil fuels have always been a concern; especially, with the unfavorable gases emitted when these fossil fuels are combusted. Hence researchers around the world are striving hard to find an alternative source which should be quite clean, or at least not hard on our environment.^{2,3} Hydrogen in this regard is termed

as the fuel of the future.⁴

Solar harvesting materials have shown a ray of hope in this case of study.⁵⁻⁸ Solar harvesting materials have already been actively involved in photocatalysis and water splitting reactions for photocatalytic hydrogen production.⁹⁻¹² The most established and well known metal oxide for water splitting is TiO₂. However a number of different metal oxides and its composites have also been reported.¹³⁻¹⁶ Different materials with various morphology, fillers, co-catalyst and techniques have been employed and manipulated to convert the solar energy efficiently.¹⁷⁻²¹ Nonetheless, in spite of employing a variety of different morphology of materials for water splitting, there is no breakthrough in increasing quantum yield (QY) yet hinting that there may be other factors playing more significant role in increasing the activity. In our opinion, synthesis strategies employed to bring various textural changes in the morphology did not seem to give appreciable enhancement in QY.²² High lifetime of charge carriers (ns to μs and higher) along with their fast utilization could be the key to enhance the efficiency to a new level, and whatever required to achieve these could be the inputs for newer synthesis strategies.

When it comes to tuning the Fermi level (EF) of the composite, different fillers, co-catalyst, dopants play an important role. In terms of fillers, recently graphene-based components have played a very important role in the photocatalytic production of hydrogen.²²⁻²³ Similarly, there are many reports where noble metals have been employed;

^a Catalysis Division, National Chemical Laboratory, Dr. Homi Bhabha Road, Pune 411 008, India. Fax: (+91) 20-2590-2633; E-mail: cs.gopinath@ncl.res.in

^b Department of Condensed Matter Physics and Materials Science, Tata Institute of Fundamental Research, 1 Homi Bhabha Road, Mumbai 400 005, India

^c Network of Institutes for Solar Energy (NISE), NCL Campus, Pune 411 008, India.

^d Centre of Excellence on Surface Science, NCL Campus, Pune 411 008, India

Electronic Supplementary Information (ESI) available: [EDX analysis and representative GC result (SI-1), HAADF-STEM image of Pt_{0.5}/Au₁/TiO₂ (SI-2) XRD patterns (SI-3), and decay profile of PCE (SI-4)]. See DOI: 10.1039/x0xx00000x

especially, metals that exhibit surface plasmon resonance (SPR) by visible light absorption, like Au and Ag, were found to play a very important role due to visible light absorption.²⁴⁻²⁶ Amongst non plasmonic active metals, Pt has been reported extensively due to its Schottky junction formation at the interfaces of Pt-TiO₂ composite, resulting in a larger barrier height than that of Au nanoparticle; in fact this reduces the rate of electron-hole (e⁻-h⁺) recombination.²⁷⁻²⁸ However, such (Pt) nanoparticle exhibits no visible light absorption, but very good catalytic activity. To take advantage of visible light absorption through SPR and to minimize the charge carrier recombination simultaneously, bimetallic nanoparticles of Au and Pt on TiO₂ would be a good strategy. Few methodologies have been adopted to achieve the above;²⁹⁻³² however, their applicability in SWS without any sacrificial agents is yet to be demonstrated. Apart from the activity aspects, the heterojunction formed at the interface of two metals is rarely investigated.

Herein, we study and investigate the photocatalytic production of hydrogen through semiconductor bimetal nanocomposite. Where Au/TiO₂ was used as the base composite, on which Au + second metal (Ag, Pt and Pd) was deposited simultaneously and used also as a co catalyst to validate the significance of Pt or any second metal. Latter the junction property is evaluated through various controlled experiment and physical characterization techniques. Due to its high activity, Pt-Au/TiO₂ was investigated extensively and the results are presented here. Present report is a part of research efforts from our laboratory to understand the SWS and related aspects.^{5,9,16,22,32} Indeed, this is our first report on bimetal systems along with overall water splitting on Au + M on TiO₂ (M = Pt, Pd and Ag).

Experimental Section

Synthesis of M-Au/TiO₂ composites (M = Ag, Pt and Pd)

P25 (100 mg) was taken in a 250 ml RB flask with 120 ml water and 30 ml methanol. This reaction mixture was purged with argon gas for 30 min. under continuous stirring. HAuCl₄.4H₂O (255 μl of 20 mM) from Sigma Aldrich was added, and after which the reaction mixture was exposed to UV light from a 400 W UV (medium pressure Hg-vapour lamp, λ = 365 and 310 nm; 240 mW/cm²) lamp for 30 mins. Subsequently, 130 μl of 20 mM H₂PtCl₆.H₂O (Sigma Aldrich) was added to the same reaction mixture and it was again exposed to UV light for 30 mins. Above Pt + Au solution makes it feasible to form bimetal (or alloy) on Au/TiO₂ surfaces. After completion of photodeposition of metal nanoclusters, the materials were thoroughly washed with double distilled water by centrifugation, and heated in the oven at 60 °C for 12 h to remove any trace amount of residual methanol and any metal ions. The collected samples were then tested for hydrogen production and other characterization. Same condition is also applied for nanocomposite synthesis based on other metal combination. Gold was deposited first, followed by any second metal deposition. Metal content was analyzed by ICP analysis.

Materials characterization

A potentiostat (Metrohm-Autolab model PGSTAT302N) was used for the electrochemical characterization using typical three electrodes (Ag/AgCl as reference, Pt and catalyst coated FTO as counter and working electrodes, respectively) assembly in a quartz beaker. 5 mg of sample was dissolved in 100 μl of ethanol; out of that 20 μl was drop-casted over 1 cm² ITO substrate by doctor blade method to make about 200 nm thick film of photocatalyst. UV-visible spectral measurements were made with Shimadzu (Model UV-2550) spectrophotometer under diffuse reflectance mode for powder sample with BaSO₄ as the reference material. Raman scattering measurements were carried out using a Horiba JY LabRAM HR 800 Raman spectrometer coupled with a microscope in reflectance mode, where a laser of 632 nm wavelength was used as an excitation source with a spectral resolution of 0.3 cm⁻¹.³³ The photoluminescence (PL) measurements were carried out using the JobinYvon-Spex make Spectrofluorometer (Fluorolog version-3; Model FL3-11) with 450 W high-pressure xenon arc lamp as an excitation source. PL excitation (λ = 350 nm) and emission spectra were acquired at room temperature at a spectral resolution of 0.2 nm at a slit width of 0.25 mm. Electron life time (Fluorescence) measurements were carried out using a Horiba Jobin Yvon Fluorolog 3 spectrophotometer equipped with a 450 W Xe lamp. Fluorescence lifetime decays were analyzed using a time-correlated single photon counting (TCSPC) setup from IBH Horiba Jobin Yvon. This is also equipped with a 375 nm diode laser (IBH, UK, Nano LED-375 L, λ_{max} = 375 nm) as a sample excitation source.

Powder x-ray diffraction (PXRD) data of catalytic materials were collected by using a PAN analytical X'pert Pro dual goniometer diffractometer. The radiation used was Cu Kα (1.5418 Å) with a Ni filter. The data were collected with a step size of 0.02° at a scan rate of 0.5°/min. The sample was rotated throughout the scan for better counting statistics. TEM analysis was carried out using TECNAI 3010 electron microscope (Cs = 0.6 mm, resolution 1.7 Å) at 300 kV. The samples for TEM analysis were prepared by casting a drop of the dilute sample dispersed in isopropanol on to a Cu grid. A FEI-TITAN microscope operated at 300 kV equipped with FEG source, Cs (spherical aberration coefficient) corrector for condenser lens systems and a high angle annular dark field (HAADF) detector was used to perform scanning transmission electron microscopic (STEM) experiments. Semi convergence angle of electron probe incident on the specimen and camera length were maintained 17.8 mrad and 128 mm respectively during the experiments and all images were taken with HAADF detector.³⁴ The SEM system equipped with an EDX attachment (FEI, model Quanta 200 3D) was used for morphological and chemical composition.³⁵ XPS measurements have been taken with a custom-built ambient pressure XPS system³⁵ (Prevac, Poland) and equipped with a VG Scienta SAX 100 emission controller monochromator using an Al Kα anode (1486.6 eV) in transmission lens mode. The photoelectrons are energy analyzed using VG Scienta's R3000 differentially pumped

analyzer. Low energy electron flood gun was employed to neutralize the static charge build-up.⁵

Hydrogen generation studies

The photocatalytic experiments involved a borosil photoreactor with a 50 ml capacity;³⁵ it is also equipped with a port for measurements of H₂ gas at regular time intervals. A known amount (20 mg) of catalyst was added to a 30 ml of distilled water and 10 ml methanol employed as a sacrificial agent. This is evacuated to 4×10^{-3} mbar pressure to remove the air present above the reaction mixture. After which, the sample was exposed to a white light illumination using a solar simulator of 300 W power (Newport solar simulator) using either AM1.5 (100 mW/cm²) or >400 nm (92 mW/cm²) filter; after every 5 h, the photoreactor was evacuated and irradiation continued to measure the activity for several cycles. Analysis was carried out at regular time intervals through a gas chromatograph (Agilent 7890A) using a HP-Molsieve column and equipped with a thermal conductivity detector (TCD). Ar at a flow rate of 25 cm³/min was used as a carrier gas. Apparent quantum yield (AQY) was calculated using the formula given below:

$$AQY (\%) = \frac{2 \times \text{Number of H}_2 \text{ Molecules}}{\text{Number of incident photons}} \times 100 \quad (1)$$

It is presumed that 21.5 % of AM1.5 filtered photons (one sun condition) are incident which corresponds to the absorption of photons from 370 to 640 nm at the rate of 3.33×10^{19} photons/s.³² We believe the above assumption is valid since nanogold is the only visible light absorber in the present set of composites, and no consideration is given for any multiple exciton or field effect due to SPR of nano gold (in the AQY calculation), although we do not want to rule out the latter's contribution to H₂ generation.

Results and discussion

Water Splitting

Different compositions of Au, and Au + Pt was synthesized and then tested for hydrogen production and the results are shown in Table 1. Numeral that follows as subscript after Au or Pt gives the weight percent of those metal. Pt/TiO₂ does not show any SWS activity under the present experimental conditions of one sun irradiation (with AM1.5 filter). However, Au/TiO₂ shows a H₂ yield of 307 μmol/h g highlighting the light harvesting by SPR of gold nanoparticles. With 0.5 wt % deposition of Pt over Au/TiO₂, the H₂ yield increased four times that of Au/TiO₂ to 1275 μmol/h g. Interestingly, double the amount of gold and Pt (Pt-Au₂/TiO₂) also led to similar, but marginally smaller amount (1228 μmol/h g) of H₂ yield, which is within the experimental uncertainty of 5 %. Nevertheless, H₂ yield decreased significantly and varied between 850 and 1100 μmol/h g for other compositions with larger amount of Au and Pt of more than 1.5 wt % (Table 1). Neither too high content of Au (5 wt. %) nor Pt (1.5 wt. %) helps in generating higher H₂ yield, than 1300 μmol/h g. In fact, larger amount of Au and Pt together is significantly counterproductive for H₂ yield. When

Au content is high (5 wt. %), the colour of the composite turns more towards black indicating the poor light absorption by the composite. An overall comparison of the results led us to consider Pt_{0.5}-Au₁/TiO₂ to be the optimum (or benchmark) catalyst composition for the best H₂ yield. The likely reason for high photocatalytic activity of Pt_{0.5}-Au₁/TiO₂ is due to a large dispersion of Pt on Au, as well as Au and Pt onto TiO₂ crystallites without reducing its light absorption capability, as shown in physico-chemical characterization studies in the following sections.

Table 1: H₂ production from SWS with different compositions of Pt-Au/TiO₂ nanocomposite with AM1.5 filtered (one sun condition) and 400 nm cut-off filtered light.

Composite Code	H ₂ yield / μmol/g.h ^a	
	AM 1.5 filter (AQY)	>400 nm (AQY)
Au ₁ /TiO ₂	307 (1.5)	66 (0.3)
Pt _{0.5} -Au ₁ /TiO ₂	1275 (6.4)	311 (1.6)
Pt ₁ -Au ₁ /TiO ₂	1091 (5.5)	251 (1.3)
Pt _{0.5} -Au ₂ /TiO ₂	854 (4.3)	119 (0.6)
Pt ₁ -Au ₂ /TiO ₂	1228 (6.1)	100 (0.5)
Pt _{1.5} -Au ₂ /TiO ₂	1035 (5.2)	97 (0.5)
Pt _{1.5} -Au ₅ /TiO ₂	916 (4.6)	88 (0.4)
Pt ₁ -TiO ₂	0	0
TiO ₂	0	0

^aH₂ yield reported varies within 10 % between two different batches of materials with the same composition.

Further, it is also to be mentioned that a sequential deposition of Au on TiO₂ followed by Pt on Au/TiO₂ (Pt/Au/TiO₂) exhibits hydrogen generation activity of not more than 820 μmol/h g. This underscores the necessity of metal deposition together towards better activity, possibly through bi-metal and/or alloy formation. SWS activity was also measured with 400 nm cut-off filter to remove small percent of photons available up to 370 nm and the results are shown in Table 1. H₂ yield decreased between 8 and 24 % compared to that of with one sun condition, suggesting a predominant contribution from the radiation below 400 nm from the simulated one sun condition. It is to be mentioned that rutile part of P25 can absorb below 405 nm, and using 400 nm cut-off filter predominantly restricts light absorption between 380 and 400 nm. This is also a reason for a large decrease in HY with 400 nm cut-off filter. Nevertheless, Pt-TiO₂ does not show any activity even with one sun condition indicating the importance of nanogold for solar harvesting; this also suggests the light absorption by TiO₂ is the limiting factor and confirms with earlier literature reports.³⁶

In view of the above results, 0.5 and 1 wt % of different second metal was co-deposited with Au on Au/TiO₂ and evaluated for SWS; 0.5 wt % of second metal shows the better activity than 1 wt %, and hence we restrict our discussions to those compositions only in the present manuscript. Different second noble metals are chosen from the same group in the periodic table, as that of either Au or Pt, such as Ag and Pd. Hydrogen yield obtained is shown in Table 2. The highest H₂ yield was found to be 1275 μmol/h g in case of Pt_{0.5}-Au₁/TiO₂,

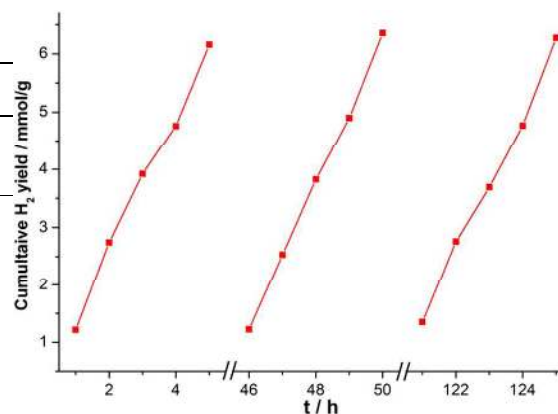
Table 2: Comparative hydrogen production of $M_{0.5}$ -Au₁/TiO₂ based nanocomposite.

Material Code	H ₂ yield (μmol/g h) AM 1.5 (AQY)
Ag _{0.5} -Au ₁ /TiO ₂	466 (2.3)
Pt _{0.5} -Au ₁ /TiO ₂	1275 (6.4)
Pd _{0.5} -Au ₁ /TiO ₂	872 (4.4)

followed by Pd_{0.5}-Au₁/TiO₂, (872 μmol/h g) and Ag_{0.5}-Au₁/TiO₂ (466 μmol/h g), under one sun condition or with 400 nm cut-off filter. As earlier, the H₂ yield decreases largely with 400 nm cut-off filter and about 1/5th of H₂ yield observed as that of AM1.5 filter. Nevertheless, among the second metals deposited and evaluated, Pd is second-best in terms of hydrogen yield. It is interesting to note that, in spite of SPR associated with nano silver (around 420 nm) in Ag_{0.5}-Au₁/TiO₂, higher H₂ yield observed with Pd_{0.5}-Au₁/TiO₂, indicating the role of Pd. It is to be noted that Pd and Pt exhibits high density of states near E_F³⁷ and this electronic factor might have a role in charge separation and utilization and it is worth exploring.

Second metal deposition over Au/TiO₂ was specifically attempted to have a possible and controlled bimetallic/alloy system as their miscibility and interface plays a significant role in catalysis as well as in photocatalysis. It is also known that certain interfaces separates the electron-hole pairs efficiently or separate and store the electrons, as many metals acts as electron sink. Above aspects minimize the charge recombination and helps towards charge utilization.

To evaluate and understand the efficacy of Pt_{0.5}-Au₁/TiO₂ in terms of photocatalytic hydrogen production, water splitting reaction (WSR) was thus performed under a simulated sunlight in an aqueous methanol solution and the results are shown in Figure 1 for twenty five cycles of 5 h each. After each cycle,

**Fig. 1** Photocatalytic H₂ evolution activity of Pt_{0.5}-Au₁/TiO₂ under one sun conditions with aqueous methanol solution. After every 5 h gaseous products are evacuated.

complete evacuation of gaseous products was made and SWS continued. Photostability has been proved by continuous usage of the catalyst for 25 cycles with consistent hydrogen production. This is another important feature towards sustainability that we encountered, which also makes it a better and potential catalyst to work with.

The molecular ratio of H₂ and CO₂ was found to be about 3±0.2 states that one molecule CH₃OH and water leads to 3 molecules of H₂ and one molecule of CO₂ in accordance with the general mechanism.³⁶ GC results shown (SI-1a in supporting information) for products analysis of SWS gives only H₂ and CO₂ and without any other partially oxidized products of methanol, such as formaldehyde, formic acid. HPLC analysis of test solution intermittently did not show any significant amount of formaldehyde or formic acid, suggesting that it is unlikely that they are present in solution.^{36b} From the

Table 3: Comparative photocatalytic hydrogen yield for Pt/Au/TiO₂ nanocomposite under variable experimental condition.

Catalyst	λ Range (photon flux)	H ₂ in μmol/g.h (AQY)	Photocatalytic medium	Ref.
Pt _{0.5} -Au ₁ /TiO ₂	450-600 nm (83 mW/cm ²)	~130 [@] (0.4)	Water/2-propanol (1:1)	[29a]
Pt _{0.5} -Au _{0.5} /TiO ₂	UV-A	~7500	Water/Ethanol (1:1)	[30]
Pt _{0.5} -Au _{0.5} /TiO ₂	>400 nm	37.5 ml/g.h	Water/Ethanol (1:1)	[30]
Pt _{0.5} -Au _{0.25} /TiO ₂	UV-Vis	~2400	Water/L-ascorbic acid (0.1 mM)	[31a]
Pt _{0.5} -Au _{0.75} /TiO ₂	420 (8 mW/cm ²) + 550 (20 mW/cm ²)	~24	Water/L-ascorbic acid (0.1 mM)	[31b]
Pt _{0.5} -Au _{0.5} /P25	UV+Vis,	17330,	Water/Methanol (9:1)	[36c]
Pt _{0.5} -Au _{0.5} /P25	>420 nm	0	Water/Methanol (9:1)	[36c]
InGaN@ZnO	> 400 nm	17-66 [#] (0.26)	Water	[32]
Pt _{0.5} -Au ₁ /TiO ₂	AM 1.5 (100 mW/cm ²)	1275 (6.4)	Water/methanol (3:1)	Present work
Pt _{0.5} -Au ₁ /TiO ₂	> 400 nm (92 mW/cm ²)	311 (1.6)	Water/methanol (3:1)	Present work
Pt _{0.5} -Au ₁ /TiO ₂	AM 1.5 (100 mW/cm ²)	162 (0.74)	Water	work

Hydrogen yield depends on the material composition.

@Hydrogen evolution rate reported was 6.5 μmol/h/50 mg in ref.29a.

Journal Name

ARTICLE

photocatalytic hydrogen production it is clearly evident that the hydrogen production yield in case of Pt_{0.5}-Au₁/TiO₂ nanocomposite increased up to 3.5 times to that of Au₁/TiO₂. However, pure TiO₂ and Pt_{0.5}/TiO₂ was found to be inactive under one sun conditions (Table 1). Such marked improvement in the photocatalytic activity of Pt_{0.5}-Au₁/TiO₂ supports the synergistic influence of Au and Pt with TiO₂ in solar light harvesting. In addition to this, the reported value of hydrogen production is also comparatively high under visible light than the existing literature as shown in Table 3. Particularly, the result reported in ref.36c is strikingly in contrast to the present findings. Although Pt-Au/P25 compositions are similar, no visible light activity was observed in ref.36c and it is attributed to the Pt acting as shell enclosing the gold core. In fact, no Au-SPR band was observed for Pt-Au/P25^{36c} indicating the method of preparation critically matters for the activity and the reaction mechanism.

The large amount of H₂ production is attributed to the electronic intimacy not only between TiO₂ framework and Pt/Au, but also between Pt and Au. In addition to the above electronic factor, catalytic activity of small Pt-clusters for hydrogen production is important. Indeed, it is the synergy between the electronic factor and catalytic activity of Pt improves the activity to a large extent. We further evaluated Pt_{0.5}-Au₁/TiO₂ for overall water splitting (OWS) without employing any sacrificial agent, such as methanol. As in Fig. 1, the OWS measurements were carried out for 5 h and evacuated before the next cycle of experiment. Three cycles of 5 h each experiment was measured and the results are consistently reproduced within an error of 5 %. Under such condition, photocatalytic hydrogen yield was found to be 162 μmol/h.g. To the best of our knowledge, there are no reports available in the literature which reports OWS in simulated sunlight with such high value for Au or Au+Pt on titania or ZnO based system. We attribute the hydrogen production from OWS due to the electronic integration of Au with Pt as well as titania, catalytically different Pt in Pt_{0.5}-Au₁/TiO₂ and detailed characterization provides more information.

To evaluate the presence of metallic nanoparticle on TiO₂ surface, EDAX measurements were carried out which indicate the presence of both metal on TiO₂ matrix (see supporting information (SI), Fig. SI-1b). Atomic percentage evaluated through EDAX also supports the metal wt. % of the nanocomposite.

TEM and HAADF-STEM imaging

To investigate the reasons for the highest hydrogen yield from Pt_{0.5}-Au₁/TiO₂, detailed characterization studies was carried out. TEM and HAADF-STEM was carried out, especially to explore

the presence of interface interaction of Pt on the surfaces of Au-particles as well as with titania. Results showed TiO₂ nanoparticles of P25 were of around 20-30 nm (Fig. 2a and c). Presence of metal particles could be identified from d-values, as shown in Figure 2b; however, all dark spots (Fig. 2a, c, d, and e) may not be due to metal or alloy species. Although Pt particles were identified easily on Pt/TiO₂ (Fig. 2d), it was hard to find distinct nanoparticle formation of Pt from Pt_{0.5}-Au₁/TiO₂, which indicates the possible miscibility of Pt with Au. Intensity of HAADF-STEM image is proportional to the square of the atomic number (*Z*²) of the elements presents in the imaged region. Since the difference between Au and Pt is 1, therefore, no observable contrast difference present between the regions enriched with of Pt and with Au, which makes it difficult to distinguish them in a single nanoparticle. Nonetheless, a distinct HAADF-STEM image of single bimetal (Au/Pt mixed) nanoparticle shown in Figure 2f reveals the different lattice fringes and inhomogeneity with lattice strain. Careful measurement of lattice fringes show the formation of a thin layer of Pt with lattice fringes belong to (111) facet (*d*₁₁₁ = 0.21 nm) (see supporting information, Fig. SI-2). Very small islands of Pt suggest a discontinuous thin Pt layer on gold nanoparticle. At certain regions clear lattice fringes belonging to Au (111) facet were observed, however, at other regions overlapping between the facets of Au and Pt nanoparticle occur and some of them are shown in yellow rectangles (Fig. SI-2).³⁸ Those green diamond region shows no clear ordering and extension of some of the nearby lattice fringes are lost, as the lattice fringe moves towards the center of the diamond shape; this severe disorder is also attributed to the overlap of Pt on Au, and it is possibly due to alloy formation. We believe such miscibility between Au and Pt and the presence of Pt on the surface constitutes to be a critical factor resulting in a high photocatalytic activity. In such case, plasmonic activity of Au nanoparticle and the high conductivity of Pt could be retained.

It is also to be mentioned that thin layer of Pt on gold nanoparticle and Pt-Au alloy should be electronically different from that of Pt in Pt/TiO₂. Indeed, the simultaneous deposition of Pt+Au procedure adopted, after deposition of 0.5 wt % gold, ensures that bimetal/alloy formation occurs. High water splitting and significant OWS activity observed with Pt_{0.5}-Au₁/TiO₂ suggesting the role of Pt is highly effective in separation of electron-hole pairs due to the availability of sensitizer and co-catalyst in a single particle. Collective oscillation of electrons or SPR due to visible light absorption by gold, should lead to local electromagnetic field enhancement and how the same influences the nearby Pt layers is not known till date. Especially those nano Pt-islands/layers that are in

contact with gold or flanked between adjacent gold layers should be under the influence of local electromagnetic field due to Au-SPR. From the high water splitting activity (Table 1-3) and photocurrent generation (Fig. 8) observed, we speculate that there could be positive influence towards increasing the charge separation as well as the catalytic activity. Small amount of Pt clusters on TiO_2 cannot be ruled out on $\text{Pt}_{0.5}\text{-Au/TiO}_2$. In addition, electronically different Pt present in $\text{Pt}_{0.5}\text{-Au/TiO}_2$

should be suppressing the backward $2\text{H}_2 + \text{O}_2 \rightarrow 2\text{H}_2\text{O}$ reaction to a significant extent, which leads to OWS reaction. Nonetheless, these aspects need to be explored in a systematic and well-controlled manner. Recent report by Maeda^{27a} on the observation of OWSR on $\text{Pt/TiO}_2(\text{R})$, but with $\lambda > 350 \text{ nm}$, indicates the window present to manipulate the activity by suppressing the backward reaction.

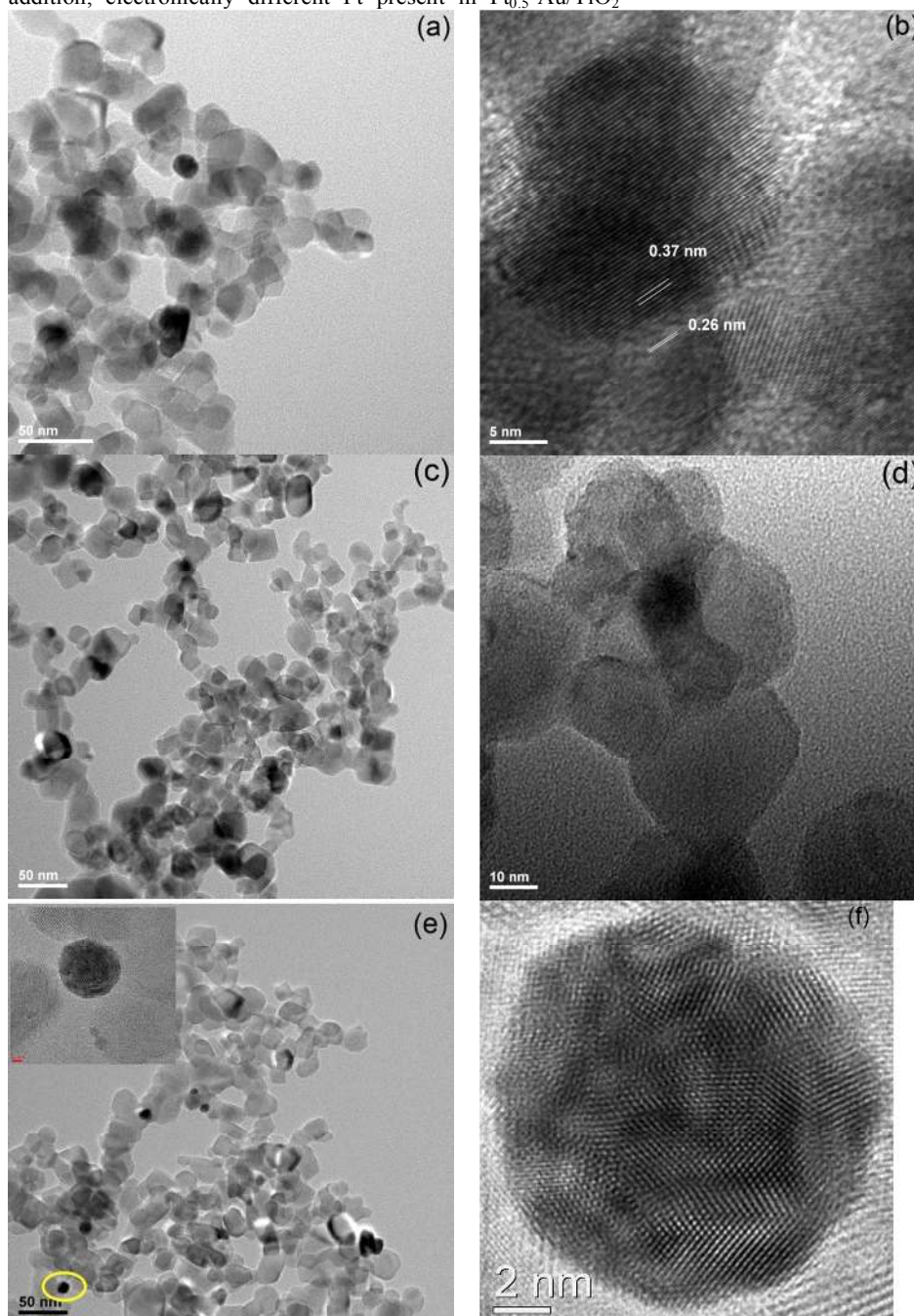


Fig. 2 HRTEM images of, (a-b) Au_1/TiO_2 , (c-d) $\text{Pt}_{0.5}/\text{TiO}_2$ and (e) $\text{Pt}_{0.5}\text{-Au}_1/\text{TiO}_2$. A spherical gold particle (indicated by yellow ellipse in (e)) is shown in the inset. (f) HAADF-STEM image of single bimetal (Au/Pt mixed) nanoparticle. See Fig. SI-2 for intermixing of Pt and Au.

UV-Visible Absorption

To explore the Au-Pt interaction, UV-visible absorption spectroscopy was measured for all four systems i.e. TiO_2 , Au_1/TiO_2 , $\text{Pt}_{0.5}/\text{TiO}_2$ and $\text{Pt}_{0.5}\text{-Au}_1/\text{TiO}_2$ and the results are shown in Figure 3. All the four materials show a major absorption cut-off at 380 nm. This reflects that metal nanoparticle does not affect the band gap of TiO_2 nanoparticle. Colour associated with relevant composite materials are shown in Figure 3 inset. On Pt deposition on titania ($\text{Pt}_{0.5}/\text{TiO}_2$), there is colour change from white to grey. This further validates the insignificant change in absorption spectra of $\text{Pt}_{0.5}/\text{TiO}_2$ to that of pure TiO_2 . On gold deposition on titania (Au_1/TiO_2), bright purple colour develops, which changes to purple-grey on Pt deposition ($\text{Pt}_{0.5}\text{-Au}_1/\text{TiO}_2$). However, Au deposition makes a drastic change in both colour and in absorption spectra as it shows purple colour with SPR absorption around 550 nm. More gold deposition turns the colour towards dark purple (Au_2/TiO_2) and then towards greyish black (Au_5/TiO_2), as shown in Figure 3. Very importantly, a blue shift of 15 nm, from 550 to 535 nm, on Pt deposition (0.25 and 0.5 wt %) on Au/TiO_2 was observed for Au-SPR feature along with a significant decrease in intensity of SPR features. SPR intensity further decreased with increase in Pt content (1 wt. %) and the resultant material gained a grey color.

Selective blue shift and decreased SPR intensity of Au feature on Pt-deposition underscores the strong possibility of Pt deposition predominantly on Au particles and a change in electronic interaction of the composite; indeed this is further supported by TEM results (Fig. 2). Above observations also highlight the electronic interaction between Pt and Au, possibly through alloy or bimetal formation.³⁹

Raman spectroscopy

Raman spectroscopy is a versatile tool to determine the structural features and electronic interaction present in the composites. Representative Raman spectra of Pt-Au/ TiO_2 composite materials are shown in Figure 4. All six fundamental Raman active features of anatase (145 (E_g), 198 (E_g), 398 (B_{1g}), 516 ($A_{1g}+B_{1g}$), and 640 cm^{-1} (E_g)) (dotted arrows in Fig. 4) and two typical rutile features are observed at 440 (E_g), 610 (A_{1g}) cm^{-1} (dashed arrows in Fig. 4) in all the cases with a quite significant difference.

E_g feature appeared at 143 cm^{-1} on TiO_2 and Pt/TiO_2 , which is in good correspondence to literature reports,⁴⁰ however it shifts to 155 cm^{-1} after nanogold or Au+Pt deposition. This shift was found to be similar in both the case of Au or Au+Pt. Although an interference in the intensity of Raman features due to SPR of gold with incident photons at 633 nm is expected, shift in Raman features necessitates the electronic interaction between titania and gold. However, no such shift was observed on Pt deposition hints the possibility of interaction should be minimum between Pt and TiO_2 in Pt/TiO_2 ; this is fully supported by literature reports and a minimum metal-support interaction has been indicated.^{40a} Significant blue shift and broadening is also observed with all Raman features upon gold deposition. For example, FWHM of E_g feature in the case of TiO_2 is 27 cm^{-1} and it doubles to 56 cm^{-1} accompanied with

peak asymmetry; critically the E_g feature itself shifts from 143 to 155 cm^{-1} on gold deposition. Finally, the asymmetry in the peak feature also originates after metal deposition, especially encountered at 640 cm^{-1} (E_g). The anatase (101) facet exhibits a

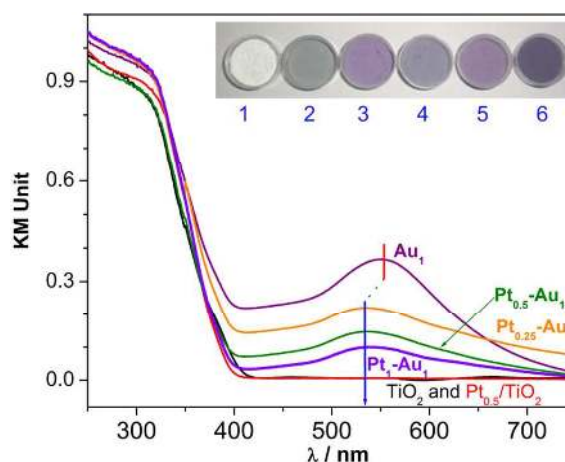


Fig. 3 UV-vis absorption spectra of TiO_2 , $\text{Pt}_{0.5}/\text{TiO}_2$, Au_1/TiO_2 , $\text{Pt}_{0.25}\text{-Au}_1/\text{TiO}_2$, $\text{Pt}_{0.5}\text{-Au}_1/\text{TiO}_2$ and $\text{Pt}_1\text{-Au}_1/\text{TiO}_2$ nanocomposite. Inset shows a digital photograph for the colour associated with composites (from 1 to 6) TiO_2 , $\text{Pt}_{0.5}/\text{TiO}_2$, Au_1/TiO_2 , $\text{Pt}_{0.25}\text{-Au}_1/\text{TiO}_2$, Au_2/TiO_2 and Au_5/TiO_2 . Au-SPR absorption maximum shifts from 550 nm on Au_1/TiO_2 to 535 nm on $\text{Pt}_{0.5}\text{-Au}_1/\text{TiO}_2$, indicating the electronic interaction between Au and Pt.

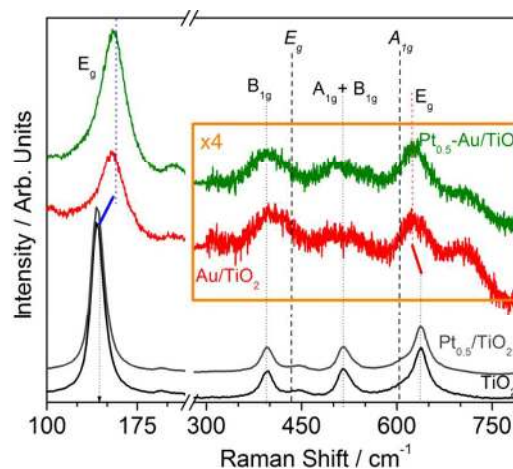


Fig. 4 Raman spectra of TiO_2 , Au_1/TiO_2 , $\text{Pt}_{0.5}/\text{TiO}_2$ and $\text{Pt}_{0.5}\text{-Au}_1/\text{TiO}_2$ composites. Rutile features are indicated by dashed line and italic font. The Raman-active E_g mode on TiO_2 at 143 cm^{-1} shows a blue shift to 155 cm^{-1} with increased line broadening, asymmetry and decreased intensity after deposition of Au and Au+Pt, indicating an electronic interaction of Au with TiO_2 . All anatase features are broadened after Au-deposition to be noted. TiO_2 and $\text{Pt}_{0.5}/\text{TiO}_2$ spectra are divided by a factor of 5, to have comparable intensity.

V-like corrugated structure with alternatively arranged five coordinated Ti (Ti^{+3}) (at trough) bound with oxygen on the edges. STM studies reported by Diebold et al^{40b} on Pt/TiO_2 and Au/TiO_2 demonstrates the preference of Pt deposition on

terrace sites of (101) facet with a high binding energy of 2.2 eV, while gold clusters predominantly deposited on defect sites, namely oxygen vacancy and edge sites. Such structural and microstructural features are amenable for charge transfer interaction between TiO₂ and metal nanoparticle, especially with gold in the present case, and capable of shifting E_g features. Blue shift observed in Raman spectra of gold containing composites suggests a strong metal-support and electronic interaction, while the same is minimum with Pt/TiO₂. Polar interaction between the two moieties is assumed to be responsible for photoexcited electron transfer.⁴⁰

Powder X-ray diffraction (PXRD) pattern of TiO₂, Au₁/TiO₂, Pt_{0.5}/TiO₂ and Pt_{0.5}-Au₁/TiO₂ is shown in Figure SI-3 (see SI). Anatase and rutile features of TiO₂ in all the composite remains sharp, indicating the crystalline nature of TiO₂. Furthermore, crystallite size calculated by Scherrer equation is found to be 7.9±0.5 nm in all the case support the deposition of the metal take place over the surface of TiO₂. No features due to metal species are observed.

Anionic gold and XPS

To further explore the electronic interaction between TiO₂ and metals, and among Pt and Au, XPS studies were performed. Ti 2p_{3/2} core level appears at 459.0±0.2 eV (not shown) for all composites and titania, indicating that Ti is present in Ti⁴⁺ oxidation state.⁴¹ Figure 5 shows the XPS results from Au 4f core levels of Au₁/TiO₂, and Pt_{0.5}-Au₁/TiO₂. Poor signal/noise ratio reflects very small amount of gold present on the surface. However, surprisingly, Au 4f_{7/2} feature appears at 83.1 eV for the as-prepared catalysts, which is lower than the typical BE observed for gold (Au⁰) at 84 eV.^{35a,42} Interestingly, the above observation indicating the state of gold is electron rich or somewhat anionic (Au^{δ-}) in nature. It is very likely that gold deposition occurs on the defect sites, particularly oxygen

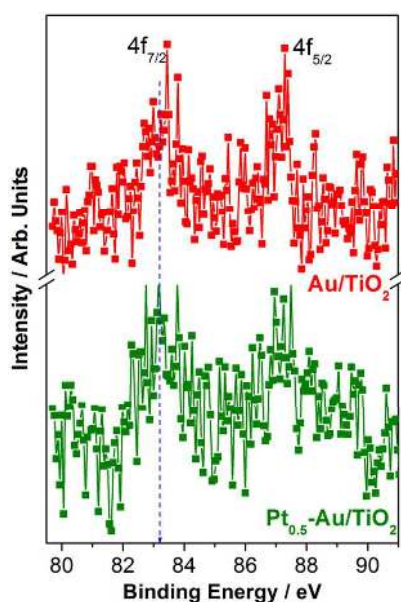


Fig. 5 XPS spectra for Au 4f core level for Au₁/TiO₂, and Pt_{0.5}-Au₁/TiO₂. Dashed line is guide to the eye.

vacancies of titania, which is electron rich.^{40b} Metal being an electron sink, there is a natural tendency for gold atoms to deposit on O-vacancy sites. Indeed, the same BE observed for Au/TiO₂ and Pt_{0.5}-Au₁/TiO₂ underscoring the observed electronic changes are predominantly due to gold. XPS results also suggest a direct electronic interaction of Au with titania and in good correspondence with results obtained from Raman spectroscopy (Fig. 4). Feasible electron transfer takes place from Au or Au + Pt nanoparticles to the TiO₂ conduction band during the photocatalysis experiments under one sun or visible light conditions.^{29,43} Our efforts to obtain meaningful Pt 4f spectra were unsuccessful.

Emission and life-time studies

Photoluminescence (PL) studies were carried out and the results are shown in Figure 6 for TiO₂ along with Au/TiO₂, Pt/TiO₂ and Pt-Au/TiO₂. Excitation wavelength employed was 350 nm. TiO₂ showed emission features between 400 and 500 nm (Figure 6). They show two similar intense and broad emission features at 416, and 438, and a shoulder around 465 nm. The emission peak at around 416 nm is due to the free exciton emission of TiO₂. Whereas, the peak at 438 nm is due to charge transfer transition from Ti³⁺ to the O²⁻ in [TiO₆]⁸⁻. Appearance of a shoulder feature at 470 nm is due to the surface state, such as Ti⁴⁺-OH.^{35a} Compared to the narrow emission features observed from anatase-phase of TiO₂,^{35a} broadening of all features indicating the emission from anatase and rutile phase at very close frequencies. Very interestingly, emission feature decreased in intensity by more than two orders of magnitude for Au₁/TiO₂, Pt_{0.5}/TiO₂ and Pt_{0.5}-Au₁/TiO₂ also shows similar emission features, but close to three orders of magnitude lower intensity compared to TiO₂. However, we attribute the decrease in emission features intensity is due to severe quenching by metal particles deposited on titania. As observed in earlier characterization results, a strong electronic interaction between Au and titania is the reason for the above quenching. Being an

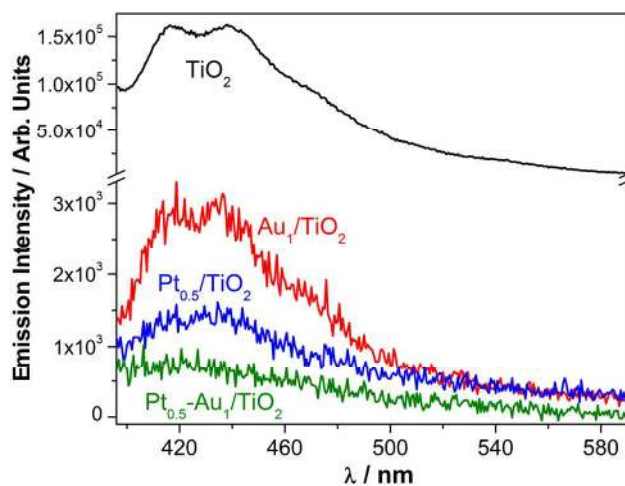


Fig. 6 PL spectra for TiO₂, Au₁/TiO₂, Pt_{0.5}/TiO₂ and Pt_{0.5}-Au₁/TiO₂ in powder form at 350 nm excitation. Note a decrease in intensity by two-three orders of magnitude by all metal deposited composites, compared to parent titania.

electron sink, Pt also leads to electron quenching, in spite of poor metal-support interaction. This quenching demonstrates the introduction of state derived from metal(s) closer to CB of titania.

No emission features from gold was observed at higher wavelengths indicating the possibility of storage of electrons in metal particles. Earlier, Chen and Murray⁴⁴ have demonstrated that Au nanoparticles possess the property of storing electrons in a quantized fashion. When TiO₂ and Au nanoparticles are in electrical contact, the photogenerated electrons are easily transferred to Au nanoparticles with UV excitation.⁴⁵ This is fully facilitated by the energy difference between them: EF of metallic Au is +0.45 V and CBmin of TiO₂ is -0.3 V versus normal hydrogen electrode potential.⁴⁵ However, this is not possible under one sun or in visible light irradiation conditions, employed in the present photocatalysis experiments, and hence EF equilibration from titania to gold is not viable. Further, the above EF equilibration condition is different from the reaction conditions. Under photocatalytic conditions reported in this communication, electrons excited into the plasmon state of gold is transferred to the CB of titania, since surface plasmon state energy is higher than the later.²⁹

Electron life time measurements were carried out to corroborate the findings from PL and the results are shown in Figure 7 for the samples TiO₂, Au₁/TiO₂, Pt_{0.5}/TiO₂ and Pt_{0.5}-Au₁/TiO₂. The materials were excited with the help of a 375 nm light-emitting diode (LED) source, and the later emission decay was recorded at 440 nm. The emission decay was found to be best fitted into a bi-exponential decay for all materials. The first decay is due to the fast radiative and Auger recombination processes; this is indeed followed by slow decay, which accounts for energy transfer mechanism. The life time analysis

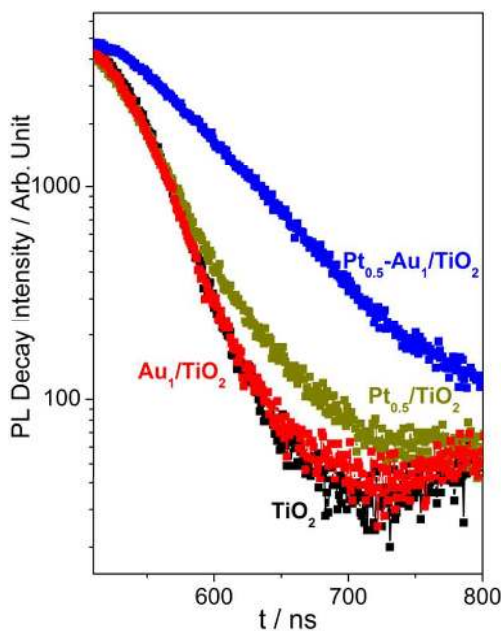


Fig. 7 Emission decay profile for TiO₂, Au₁/TiO₂, Pt_{0.5}/TiO₂ and Pt_{0.5}-Au₁/TiO₂. The excitation and monitored wavelength are 375 and 440 nm, respectively.

carried out with a bi-exponential function shows an average lifetime of 270, 320, 610, and 660 ps for TiO₂, Au₁/TiO₂, Pt_{0.5}/TiO₂ and Pt_{0.5}-Au₁/TiO₂, respectively. The average lifetime increased significantly in the cases of Pt_{0.5}/TiO₂ and Pt_{0.5}-Au₁/TiO₂, compared to TiO₂, due to increased electron-hole charge separation and electron trapping by Pt. A cursory look at the decay profiles demonstrates an increase in percent charge carriers at high life time, only after Pt deposition on either TiO₂ or Au/TiO₂. Only a marginal increase in charge carriers with high life time on Au/TiO₂ compared to TiO₂, hints the charge separation role of gold is not as that of Pt. Pt in Au+Pt alloy/bimetal allows the physical proximity, which enhances charge separation from gold also and hence a high lifetime was observed in this composite. These results corroborate well with PL results (Fig. 6), where the emission intensity from titania features decreased by 2-3 orders of magnitude upon Au, Pt or Au+Pt deposition onto P25. Above observations directly demonstrate the energy transfer by quenching from P25 to metal particles in an effective manner.⁴⁶

For further understanding of origins of photocatalytic activity, photo-electrochemical measurement (PEC) was carried out using three electrodes assembly in 0.5 M KOH electrolyte. Photo-responsive material was casted on FTO coated glass facing towards light illumination. To study the instantaneous photoresponse of materials, chronoamperometry (at 0 V vs Ag/AgCl), and linear sweep voltammetry (LSV) (-0.15 - 0.7 V at 5 mV/sec) measurements was carried out and the results are shown in Fig. 8. Two types of light response was tested, namely UV (400 W medium-pressure Hg vapor lamp, 240 mW/cm²) and AM 1.5 (solar simulator of 300 W power and 100 mW/cm² illumination) white light to follow the photocurrent change and the effect of different metal semiconductor junction. The photocurrent generated values shows easily an order of magnitude less in white light than in UV light (Fig. 8a) due to no UV in the AM1.5 filtered light (Fig. 8b). In UV, the current response to light is least in case of TiO₂ followed by Au₁/TiO₂, Pt_{0.5}/TiO₂ and Pt_{0.5}-Au₁/TiO₂. These observations and the SWS results demonstrate the necessity to utilize the small amount of UV present (4-5 %) in the solar radiation (or one sun condition) to maximize the solar harvesting. Further, three (1.5) times higher current observed with Pt/TiO₂ (Au/TiO₂) than TiO₂ underscores the effective (significant) charge separation by Pt (Au).

We have also carried out fitting a bi-exponential function to decay i-t profile with two time constants.⁴⁷

$$Y(t) = A_0 + A_1 e^{-t/\tau_1} + A_2 e^{-t/\tau_2} \quad (2)$$

$$\tau_m = \frac{\tau_1 \tau_2}{(\tau_1 + \tau_2)} \quad (3)$$

τ_m is the harmonic life time and was found to be 870, 570, 370 and 330 ps for TiO₂, Au₁/TiO₂, Pt_{0.5}/TiO₂ and Pt_{0.5}-Au₁/TiO₂ respectively (fitted curves given in supporting information, Fig. SI-4). Decrease in decay time suggests the possibility of the reduced surface trap states due to the presence of Au-Pt nanoparticle thus reducing the e⁻ - h⁺ recombination from TiO₂ to Pt-Au/TiO₂.⁴⁷

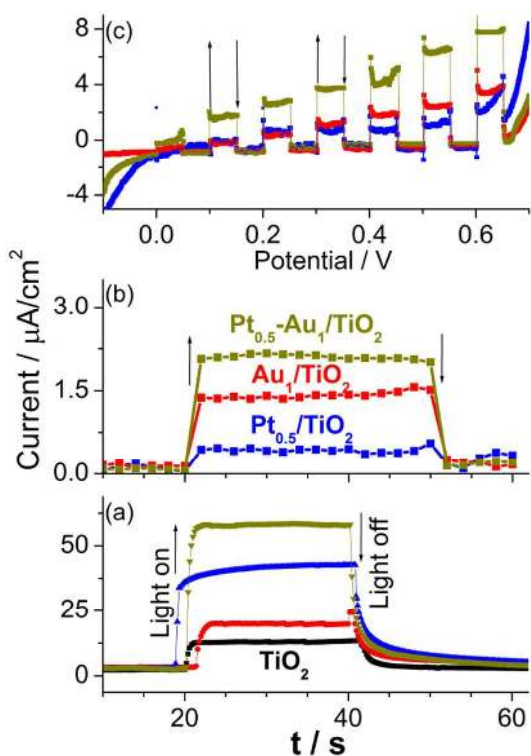


Fig. 8 Chronoamperometry measured at 0 V with, (a) UV light, and (b) AM1.5 irradiation. (c) LSV measured at a scan rate of 5 mV/s under AM1.5 irradiation for Au₁/TiO₂, Pt_{0.5}/TiO₂ and Pt_{0.5}-Au₁/TiO₂. Light on and off is indicated by up and down arrow, respectively.

In contrary to the UV light irradiation, AM 1.5 light shows some different trend. In this case also least photocurrent is observed in case of Pt_{0.5}/TiO₂, followed by Au₁/TiO₂, and Pt_{0.5}-Au₁/TiO₂ (Fig. 8b). However, TiO₂ alone was found to be totally inactive in AM1.5 light (result not shown). While Pt_{0.5}/TiO₂ do not show any water splitting activity in AM1.5 filtered light, it shows some marginal current production (0.37 $\mu\text{A}/\text{cm}^2$) in chronoamperometry. While the possibility of 4 % UV absorption (under one sun condition) by P25 is not ruled out in either case, no water splitting is attributed to the kinetic control in H₂ generation.

The trend for Pt_{0.5}/TiO₂ and Au₁/TiO₂ got reversed in AM 1.5 to that of UV light irradiation. As AM1.5 contains only simulated sunlight, which is helpful for plasmonic activity, thus makes Au₁/TiO₂ more active in PEC measurements. LSV of the four samples also follow the same trend of current response (Fig. 8c). Significant current response started in case of Pt_{0.5}/TiO₂ at about 0.1 V. The same was found at 0 V in case of Au₁/TiO₂, and Pt_{0.5}-Au₁/TiO₂. At higher applied voltage, the photocurrent generated by Pt_{0.5}-Au₁/TiO₂ doubles that of Au₁/TiO₂. A significant enhancement in current for Pt_{0.5}-Au₁/TiO₂, in comparison to Au₁/TiO₂, supports the higher photocatalytic activity in SWS. In spite of a decrease in the extent of SPR (Fig. 3) with Pt_{0.5}-Au₁/TiO₂ compared to Au₁/TiO₂, an enhancement in photocurrent generation in LSV, chronoamperometry and the highest H₂ yield in SWS underscores the role of Pt in suppressing the charge carrier

recombination and hence an enhancement in activity. All these observations suggest the charge separation and electron storage character by Pt is superior to Au, hence the longer lifetime of charge carriers (Fig. 7) and high current density for Pt_{0.5}/TiO₂ than Au₁/TiO₂ in chronoamperometry (Fig. 8a) with UV light. It is also to be emphasized the largest H₂ yield obtained in Pt_{0.5}-Au₁/TiO₂ than Au₁/TiO₂, highlighting the utilization of stored electrons for reduction of protons to hydrogen and underscoring the catalytic character of Pt.

Based on the photocatalysis experiments carried out on different catalysts and conditions, materials characterization results through different spectroscopy and structural techniques, PEC measurements under UV and visible light, a possible mechanism of water splitting is proposed in Figure 9. Under one sun conditions, photo-excitation takes place due to SPR character of Au in Au/TiO₂ or Pt-Au/TiO₂.

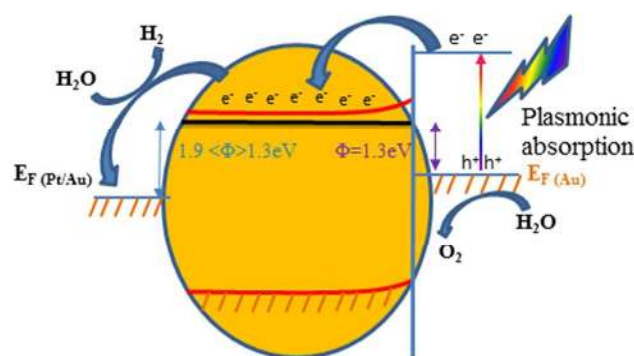


Fig. 9 Schematic energy-band diagram for Pt_{0.5}-Au₁/TiO₂ heterojunctions. EF, Φ denote the Fermi level and Schottky barrier height (in eV). Schottky barrier height of 1.3-1.9 eV is predicted for Pt_{0.5}-Au₁/TiO₂. Direct electron-hole pair separation is also possible at the Au-Pt alloy surfaces, which makes the lifetime longer for holes.

After photoexcitation, charge separation occurs due to Schottky barrier between Au and TiO₂ in Au/TiO₂; in addition to the above, effective charge separation and storage occurs by Pt in Pt-Au/TiO₂ case. Schottky barrier height for Pt-Au bimetal case should be between that of Au (1.3 eV) and Pt (1.9 eV),⁴⁸⁻⁴⁹ when the metal is just present on titania surfaces. However, EF equilibration that occurs in the composite, due to photodeposition preparation method adopted, not only makes the composite integrated electronically, but also makes the energy of SPR state of gold, CB of titania and EF of Pt to be equilibrated, specifically at interfaces. This makes the charge separation and storage significantly easier and hence higher lifetime of charge carriers, which helps for water splitting. Pt being a better co-catalyst than Au, hydrogen generation is predominant on Pt.

Conclusions

We have successfully synthesized Pt-Au/TiO₂ nanocomposite by selective synthetic strategy for the

development of higher and sacrificial agent free hydrogen production under optimum composition. Combination of Au and Pt is demonstrated for their dual property related to plasmonic absorption as well as efficient electron trap. The resultant nanocomposite exhibits strong electronic interaction between TiO₂ and Pt/Au nanoparticle and it is directly supported by Raman, UV-vis, XPS and life time analysis. Compositional and morphological analysis revealed uniform dispersion of metal nanoparticle on TiO₂ matrix and mixed phase (alloy and bimetallic) formation in Pt/Au nanoparticle. Under such scenario, the resultant nanocomposite could able to show visible light activity using visible light with a 400 nm cut-off filter along with higher H₂ yield even in the absence of methanol. To our knowledge, this is the first study which delivers the information about the visible light hydrogen production with pure water. Thus current study open the path of photocatalytic hydrogen production by using fully natural resources i.e. water and sun light. The work related to further enhancement in hydrogen production in pure water is underway for its use in large scale hydrogen production.

Present findings also insist on utilizing 4-5 % UV light present in the one sun condition to enhance the solar harvesting aspects. Large difference observed in H₂ yield with AM1.5 and 400 nm cut-off filtered radiation underscores the need to utilize the UV radiation for SWS. In total contrast to the present findings, water splitting was observed with Au-Pt alloyed TiO₂, but in UV+visible light, and no H₂ production was observed in the visible light.^{36c} Different activity reported by different groups in Table 3 for comparable Au-Pt/TiO₂ compositions underscores a significant to large difference in materials characteristics. This aspect needs to be addressed.

Although overall water splitting observed on Pt-Au/TiO₂ nanocomposites, the hydrogen yield observed to be far less to make any impact for any practical applications. A possible way to increase the hydrogen yield further is to increase the extent of noble metals content, but without increasing the particle size. This would minimize the charge carrier recombination and enhance the utilization of charge carriers, as the distance between redox sites and charge generation sites decreases. New synthesis strategies may be formulated in this direction.

Acknowledgements

We acknowledge the financial support from CSIR, New Delhi through NWP0056 project under TAPSUN program.

- 1 L. Schlapbach, A. Züttel, *Nat. Mater.* 2001, **414**, 353
- 2 T. J. Wong, F. J. Lim, M. Gao, G. H. Lee, G. W. Ho *Catal. Sci. Technol.* 2013, **3**, 1086.
- 3 P. Cheng, Z. Yang, H. Wang, W. Cheng, M. Chen, W. Shangguan, G. Ding *Int. J. Hydrogen Ener.* 2012, **37**, 2224.
- 4 K. Maeda, A. K. Xiong, T. Yoshinaga, T. Ikeda, N. Sakamoto, T. Hisatomi, M. Takashima, D. L. Lu, M. Kanehara, T. Setoyama, T. Teranishi, K. Domen *Angew. Chem. Int. Ed.* 2010, **49**, 4096.
- 5 (a) S. RajaAmbal, K. Sivaranjani, C. S. Gopinath, *J. Chem. Sci.* 2015, **127**, 33. (b) K. Sivaranjani, S. RajaAmbal, T. Das, K. Roy, S. Bhattacharyya, C. S. Gopinath *ChemCatChem* 2014, **6**, 522.
- 6 X. Xu, C. Random, P. Efstathiou, J. T. S. Irvine *Nat. Mater.* 2012, **11**, 595.

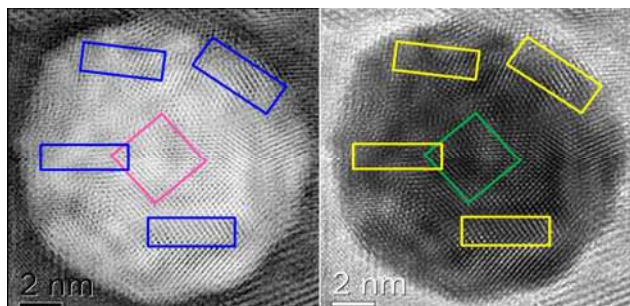
- 7 (a) A. L. Linsebigler, G. Lu, J. T. Yates *Chem. Rev.* 1995, **95**, 735. (b) M. R. Gholipour, C-T. Dinh, F. Béland, T-O. Do, *Nanoscale*, 2015, **7**, 8187.
- 8 W. J. Youngblood, S.-H. A. Lee, K. Maeda, T. E. Mallouk *Acc. Chem. Res.* 2009, **42**, 1966.
- 9 K. Sivaranjani, C. S. Gopinath *J. Mater. Chem.* 2011, **21**, 2639.
- 10 J. M. Lee, J. L. Gunjaker, Y. Ham, I. Y. Kim, K. Domen, S.-J. Hwang *Chem. Eur. J.* 2014, **20**, 17004.
- 11 H. Wender, R. V. Gonçalves, C. Sato, B. D. Maximiliano, J. M. Zapata, L. F. Zagonel, E. C. Mendonça, S. R. Teixeira, F. Garcia *Nanoscale* 2013, **5**, 9310.
- 12 (a) M. Sathish, B. Viswanathan, R. P. Viswanah, C. S. Gopinath *Chem. Mater.* 2005, **17**, 6349. (b) M. Sathish, R. P. Viswanah, C. S. Gopinath *J. Nanosci. Nanotech.* 2009, **9**, 423.
- 13 A. Fujishima, T. N. Rao, D. A. Tryk *J. Photoch. Photobio. C* 2000, **1**, 1.
- 14 Á. Valdés, J. Brillet, M. Grätzel, H. Gudmundsdóttir, H. A. Hansen, H. Jónsson, D. F. P. Klüpfel, G.-J. Kroes, F. L. Formal, I. C. Man, R. S. Martins, J. K. Nørskov, J. Rossmeisl, K. Sivula, A. Vojvodicf, M. Zächg *Phys. Chem. Chem. Phys.* 2012, **14**, 49.
- 15 M. Mapa, K. S. Thushara, B. Saha, P. Chakraborty, C. M. Janet, R. P. Viswanath, C. M. Nair, K. V. G. K. Murti C. S. Gopinath *Chem. Mater.* 2009, **21**, 2973.
- 16 S. Kumarsrinivasan, S. Agarkar, S. B. Ogale, C. S. Gopinath *J. Phys. Chem. C* 2012, **116**, 2581.
- 17 B. Hu, F. Cai, H. Shen, M. Fan, X. Yan, W. Fan, L. Xiaoa, W. Shi *Cryst. Eng. Commun.* 2014, **16**, 9255.
- 18 H. Pang, C. Wei, X. Li, G. Li, Y. Ma, S. Li, J. Chen, Zhang, *Sci. Rep.* 2013, **4**, 3577.
- 19 G. Yang, W. Yan, Q. Zhang, S. Shen, S. Ding *Nanoscale* 2013, **5**, 12432.
- 20 N. Lakshminarasimhan, A. D. Bokare, W. Choi, *J. Phys. Chem. C* 2012, **116**, 17531.
- 21 R. Asahi, T. Morikawa, T. Ohwaki, K. Aoki, Y. Taga *Science* 2001, **293**, 269.
- 22 P. A. Bharad, K. Sivaranjani, C. S. Gopinath, *Nanoscale* 2015, **7**, 11206.
- 23 (a) Q. Xiang, J. Yu, M. J. Jaroniec *J. Am. Chem. Soc.* 2012, **134**, 6575. (b) S. Bag, K. Roy, C. S. Gopinath, C. Retna Raj, *ACS Appl. Mater. Interfaces* 2014, **6**, 2692.
- 24 Z. W. Seh, S. Liu, M. Low, S.-Y. Zhang, Z. Liu, A. Mlayah, M.-Y. Han *Adv. Mater.* 2012, **24**, 2310.
- 25 (a) M. Murdoch, G. I. N. Waterhouse, M. A. Nadeem, J. B. Metson, M. A. Keane, R. F. Howe, J. Llorca, H. Idriss *Nat. Chem.* 2011, **3**, 489. (b) F. Gartner, S. Losse, A. Boddien, M.-M. Pohl, S. Denurra, H. Junge, M. Beller, *ChemSusChem* 2012, **5**, 530.
- 26 (a) H. Yuzawa, T. Yoshida, H. Yoshida *Appl. Catal., B* 2012, **115–116**, 294–302. (b) C. G. Silva, R. Juarez, T. Marino, R. Molinari, H. Garcia *J. Am. Chem. Soc.* 2011, **133**, 595.
- 27 (a) K. Madea *Catal. Sci. Tech.* 2014, **4**, 1949. (b) D. Tsukamoto, A. Shiro, Y. Shiraishi, Y. Sugano, S. Ichikawa, S. Tanaka, T. Hirai *ACS Catal.* 2012, **2**, 599.
- 28 (a) C. Zhao, H. Luo, F. Chen, P. Zhang, L. Yi, K. You *Energy Environ. Sci.* 2014, **7**, 1700. (b) Z. Jiang, J. Zhu, D. Liu, W. Wei, J. Xie, M. Chen *Cryst. Eng. Commun.* 2014, **16**, 2384.
- 29 (a) A. Tanaka, S. Sakaguchi, K. Hashimoto, H. Kominami *ACS Catal.* 2013, **3**, 79. (b) A. Tanaka, K. Hashimoto, H. Kominami *J. Am. Chem. Soc.* 2014, **136**, 586.
- 30 A. Gallo, M. Marelli, R. Psaro, V. Gombac, T. Montini, P. Fornasiero, R. Pievo, V. D. Santo *Green Chem.* 2011, **14**, 330.
- 31 (a) Z. Zhang, Z. Wang, S.-W. Cao, C. Xue *J. Phys. Chem. C* 2013, **117**, 25939. (b) Z. Zhang, A. Li, S. W. Cao, M. Bosman, S. Li, C. Xue, *Nanoscale* 2014, **6**, 5217.
- 32 (a) S. Rajaambal, M. Mapa, C. S. Gopinath *Dalton Trans.* 2014, **43**, 12546. (b) S. Rajaambal, A. K. Yadav, S. N. Jha, D. Bhattacharyya, C. S. Gopinath *Phys. Chem. Chem. Phys.* 2014, **16**, 23654.
- 33 M. Mapa, C. S. Gopinath *Chem. Mater.* 2009, **21**, 351.

ARTICLE

Nanoscale

- 34 T. Das, P. Kulkarni, S. C. Purandare, H. C. Barshilia, S. Bhattacharyya, P. Chowdhury, *Sci. Rep.* 2014, **4**, 5328.
- 35 (a) P. Devaraji, N. K. Sathu, C. S. Gopinath *ACS Catal.* 2014, **4**, 2844. (b) M. Mapa, K. Sivaranjani, D. S. Bhange, B. Saha, P. Chakraborty, A. K. Viswanath, C. S. Gopinath, *Chem. Mater.* 2010, **22**, 565. (c) K. Roy, C. S. Gopinath, *Anal. Chem.* 2014, **86**, 3683.
- 36 (a) M. Bowker, *Green Chem.* 2011, **13**, 2235. (b) G. N. Nomikos, P. Panagiotopoulou, D. I. Kondarides, X. E. Verykios *Appl. Catal. B: Environ.* 2014, **146**, 249. (c) F. Wang, Y. Jiang, D. J. Lawes, G. E. Ball, C. Zhou, Z. Liu, R. Amal, *ACS Catal.* 2015, **5**, 3924.
- 37 (a) C. S. Gopinath, K. Roy, S. Nagarajan *ChemCatChem* 2015, **7**, 588. (b) K. Thirunavukkarasu, K. Thirumoorthy, J. Libuda, C. S. Gopinath, *J. Phys. Chem. B* 2005, **109**, 13272.
- 38 C. A. García-Negrete, T. C. Rojas, B. R. Knappett, D. A. Jefferson, A. E. H. Wheatley, A. Fernández *Nanoscale* 2014, **6**, 11090.
- 39 G. Dea, C. N. R. Rao *J. Mater. Chem.* 2005, **15**, 891.
- 40 (a) J. Shi, J. Chen, T. Chen, Y. Lian, X. Wang, C. Li *J. Phys. Chem. C* 2007, **111**, 693. (b) X-Q. Gong, A. Seeloni, O. Dulub, P. Jacobson, U. Diebold *J. Am. Chem. Soc.* 2008, **130**, 370. (c) T. Ohsaka, F. Izumi, Y. J. Fujiki *Raman Spectrosc.* 1978, **7**, 321. (d) A. Fujishima, X. Zhang, D. A. Tryk *Surf. Sci. Rep.* 2008, **63**, 515.
- 41 (a) D. G. Kulkarni, A. V. Murugan, A. K. Viswanath, C. S. Gopinath, *J. Nanosci. Nanotech.* 2009, **9**, 371. (b) B. Naik, K. M. Parida, C. S. Gopinath, *J. Phys. Chem. C* 2010, **114**, 19473.
- 42 (a) S. Arrii, F. Morfín, A. J. Renouprez, J. L. Rousset, *J. Am. Chem. Soc.* 2004, **3**, 13. (b) A. Pandisamy, K. Sivaranjani, C. S. Gopinath, R. Ramaraj *RSC Adv.* 2013, **3**, 13390. (c) K. Roy, C. P. Vinod, C. S. Gopinath *J. Phys. Chem. C* 2013, **117**, 4717.
- 43 R. Su, R. Tiruvalam, A. J. Logsdail, Q. He, C. A. Downing, M. T. Jensen, N. Dimitratos, L. Kesavan, P. P. Wells, R. Bechstein, H. H. Jensen, S. Wendt, R. A. Catlow, C. J. Kiely, G. J. Hutchings, F. Besenbacher, *ACS Nano* 2014, **8**, 3490.
- 44 S. Chen, R. W. Murray *J. Phys. Chem. B* 1999, **103**, 9996.
- 45 V. Subramanian, E. E. Wolf, P. V. Kamat, *J. Am. Chem. Soc.* 2004, **126**, 4943.
- 46 (a) T. K. Sung, J. H. Kang, D. M. Jang, Y. Myung, G. B. Jung, H. S. Kim, C. S. Jung, Y. J. Cho, J. Park, C.-L. Lee *J. Mater. Chem.* 2011, **21**, 4553. (b) A. Saha, S. Chattopadhyay, T. Shibata, R. Viswanatha *J. Mater. Chem. C* 2014, **2**, 3868.
- 47 Y.-C. Pu, G. Wang, K.-D. Chang, Y. Ling, Y.-K. Lin, B. C. Fitzmorris, C.-M. Liu, J. Lu, Y. Tong, J. Z. Zhang, Y.-J. Hsu, Y. Li *Nano Lett.* 2013, **13**, 3817.
- 48 P. K. Dharani, M. V. Shankar, M. K. Murikinati, G. Sadanandam, B. Srinivas, V. Durgakumari *Chem. Commun.* 2013, **49**, 9443.
- 49 D. Tsukamoto, A. Shiro, Y. Shiraishi, Y. Sugano, S. Ichikawa Tanaka, S.; Hirai, T. *ACS Catal.* 2012, **2**, 599.

TOC



Pt-Au alloy/bimetal formation with Au deposited on O-vacancy on TiO₂ enhances overall solar water splitting with an AQY of 0.8 %.